

FULL PAPER

Open Access



# Shallow hydrothermal reservoir inferred from post-eruptive deflation at Ontake Volcano as revealed by PALSAR-2 InSAR

Shohei Narita<sup>1\*</sup>  and Makoto Murakami<sup>2</sup>

## Abstract

In 2014, a phreatic eruption occurred at the Ontake Volcano in Central Japan causing multiple deaths and missing persons. Interferometric Synthetic Aperture Radar data showed local-scale subsidence around the newly created eruptive vents after the eruption. Source modeling resulted in a nearly spherical deflation source emplaced at a depth of 500 m below the vents reflecting post-eruptive depressurization in a shallow hydrothermal reservoir. The cumulative deflation volume reached  $7 \times 10^5 \text{ m}^3$  3 years after the eruption. Comparison between our source model and GNSS data indicates that this shallow reservoir could have formed by 2007 and remained stable until the 2014 eruption. The absence of significant syn-eruptive subsidence indicates that the shallow reservoir was not the main water source driving the phreatic eruption. Under simple assumptions, mass balance between the shallow reservoir and the discharge plume from the vents indicates most of the water contained in the plume comes from greater depth than the shallow reservoir. To constrain the post-eruptive process, it is necessary to track not only deformation but also plume discharge for 3 years after the eruption.

**Keywords:** Phreatic eruption, Post-eruptive subsidence, Ground deformation, Mass balance, SAR, Volcanic–hydrothermal system, Ontake Volcano

## Introduction

Phreatic eruptions sometimes cause human fatalities when they occur in close proximity to populated areas. Such disasters might be mitigated by advanced predictions of eruption. However, in contrast to magmatic eruptions, the precursors to phreatic eruptions are minute and only appear in small proximal areas (Rouwet et al. 2014). This makes prediction challenging. It is also difficult to clarify the structure of the subsurface hydrothermal system, which is a prerequisite for developing prediction strategies. On the other hand, some very active hydrothermal systems occasionally reveal their activity through detectable geophysical signals. Such manifestations present a valuable opportunity to gain insights into the hydrothermal systems at the root of

potential calamities. There are examples where ground deformation due to mass discharge or the subsurface migration of hot fluids has been detected at volcanic–hydrothermal systems that can cause phreatic eruptions (e.g., Nakaboh et al. 2003; Maeda et al. 2017; Doke et al. 2018; Miller et al. 2018; Kobayashi et al. 2018). A number of authors have also discussed the behavior of volcanic–hydrothermal systems during non-eruptive unrest events using ground deformation data, gravity changes, geomagnetic changes, and heat flux changes (e.g., Fournier and Chardot 2012; Ingebritsen et al. 2015; Currenti et al. 2017; Tanaka et al. 2017).

Fewer studies specifically focus on the sub-decadal depressurization process following a phreatic eruption. Lu et al. (2002) detected a subsidence source at a shallow depth in Kiska Island using Synthetic Aperture Radar interferometry (InSAR) data. They speculated that vigorous steam discharge caused a decrease in the pore fluid pressure within a shallow hydrothermal system and subsidence of the ground surface. Hamling et al. (2016)

\*Correspondence: [narinari@eis.hokudai.ac.jp](mailto:narinari@eis.hokudai.ac.jp)

<sup>1</sup> Department of Natural History Sciences, Graduate School of Science, Hokkaido University, N10W8, Kita-ku, Sapporo, Hokkaido 060-0810, Japan  
Full list of author information is available at the end of the article

presented InSAR results that showed 3-year-long local subsidence after a phreatic eruption at Tongariro Volcano in 2012. They concluded that the subsidence source was a hydrothermal reservoir emplaced just beneath low-conductivity zones that were regarded as the low permeability sealing layer. Likewise, Nakaboh et al. (2003) discussed the relationship between deflation and steam discharge after a phreatic eruption in 1995 at Kuju Volcano. They showed a clear temporal correlation between the temporal vapor mass flux and deflation rate, indicating that the post-eruptive deflation was caused by steam discharge from a deflating reservoir. They concluded that a large portion of the discharged steam originated deeper than the deflation source by comparing the total discharge mass with the mass loss calculated from the decreased volume. Thus, geophysical data obtained during and after eruptive events give us the opportunity to derive important insights about hydrothermal systems that would be otherwise unobtainable.

Evolving post-eruptive ground deformation has been also observed around the eruptive crater region of Ontake Volcano in Central Japan following the 2014 phreatic explosion (Yamaoka et al. 2016). A manifestation of the deflation appeared as a decrease in the distance between the GNSS stations spanning the volcano

(Fig. 1). Likewise, multi-directional InSAR analysis using data from the Advanced Land Observing Satellite-2/ Phased Array type L-band Synthetic Aperture Radar-2 (ALOS-2/PALSAR-2) indicated evolving deflation on the summit region of the volcano. The purpose of this study is to clarify the relationship between the ongoing deflation indicated by the InSAR data and the 2014 eruption.

### Ontake Volcano eruptive history

Ontake Volcano, Central Japan, is the second highest (3067 m above sea level) stratovolcano in the country. Historically, four phreatic eruptions (1979, 1991, 2007, and 2014) have been identified. All of the eruptions are presumably linked to an underlying volcanic hydrothermal system beneath the Jigokudani Valley (Fig. 1) that has a nest of eruptive vents of recent explosions and persistent (at least 300 years) hydrothermal activity (Oikawa 2008). The magnitude of the eruptions has been uneven; the 1979 and 2014 eruptions were significantly larger than the other two events. The total mass of lithic material extruded during the 2014 eruption was 0.89–1.2 million tons, an amount on the same order of magnitude as the 1979 eruption (1.9 million tons) (Takarada et al. 2016).

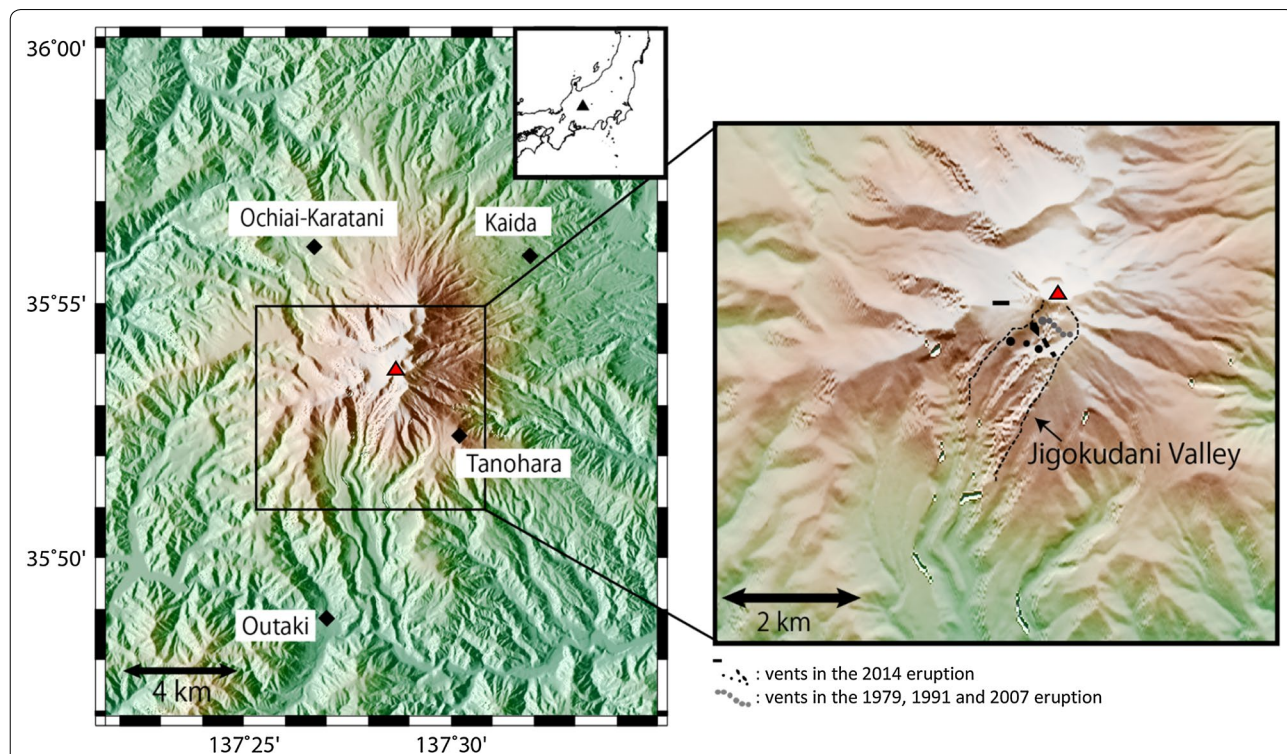


**Fig. 1** Map of the study area. The inset is a close view of the summit area and corresponds to the area of interferograms (Figs. 3, 4) and modeling (Fig. 5). Most of the hydrothermal activity at the Ontake Volcano occurs around the Jigokudani Valley (indicated with the dashed line). The black diamonds indicate GNSS stations deployed around the edifice of the Ontake Volcano. Eruptive vents are also marked

The 2007 and 2014 eruptions were observed by modern monitoring networks to detect ground deformation and seismicity. Several authors discussed the 2007 eruption using the data of these observation networks (e.g., Nakamichi et al. 2009). GNSS data indicated that a magmatic dike intruded at a depth of 8–13 km below the surface (Takagi and Onizawa 2016). Seismic data suggested that heat supplied from the magmatic intrusion may have reached the shallow hydrothermal system at depth of 1–3 km. The stimulated fluid in the shallow hydrothermal system was considered to be the direct cause of the unrest events, including the Long-Period (LP) swarms, Very Long-Period (VLP) earthquakes (Nakamichi et al. 2009) and inflation rooted at a depth of 1 km below the surface (Takagi and Onizawa 2016).

Quiescence followed, until eruptive activity started on September 27, 2014, with a few precursory phenomena (Kato et al. 2015). A rapid increase in the number of volcano tectonic (VT) earthquakes appeared 2 weeks prior to the eruption and reached 100 counts/day. Rapid upward migration of VT hypocenters toward the surface started only 10 min before the eruption. Distinct tilt change was also observed 7 min prior to the eruption at a station 3 km away from the eruption center (Maeda et al. 2017). Around the Jigokudani Valley, several vents were newly created in close vicinity to the 1979 vents but slightly shifted to the southwest.

Studies using data acquired during the 2014 event revealed important information regarding the hydrothermal systems at different depths (1–6 km). Mineralogical analysis suggested that the 2014 eruption was phreatic, because no juvenile materials were found (Minami et al. 2016). Analysis of hydrothermally altered minerals in the deposit suggested that the minerals came from a shallow depth (~ 1 to 2 km) and had been formed at temperatures below 250 °C (Minami et al. 2016). Volcanic gas observation after the eruption indicated that discharge of magmatic fluids continued during at least 2 months after the eruption with the SO<sub>2</sub> flux rapidly decreasing from 2500 to 130 ton/day between September 28, 2014, and November 21, 2014. After this period, the gas composition reflected degassing from an underlying volcanic–hydrothermal system (Mori et al. 2016).

The geophysical observations also provided significant data. The tilt change 7 min prior to the eruption was explained as the opening of a vertical crack source at 1.1 km depth beneath the Jigokudani Valley, and this opening was interpreted as inflation due to rapid boiling of liquid water (Maeda et al. 2017). The rapid upward migration of the VT hypocenters that began 10 min prior to the eruption at 3 km depth was interpreted as the swift ascent of fluid, causing propagation of crack failures along the flow path (Kato et al. 2015). A subsidence

source at a depth of 6 km was also identified from leveling surveys spanning 2009–2014 (Murase et al. 2016).

The ongoing localized subsidence around the summit region during the post-eruptive period has not previously been discussed in the context of the overall the 2014 eruption processes. This study attempts to clarify the origin of the subsidence following the eruption and its role in the overall eruption process.

### InSAR analysis

We applied interferometry to L-band SAR images acquired by ALOS-2 over Ontake Volcano between 2014 and 2017 (Fig. 2). For all the InSAR processing procedures, we used the RINC software package (Ozawa et al. 2016). The spatial averaging window (multilook) size was selected to ensure that the ground spacing of the neighboring pixels was about 20 m after rearrangement. Topographic corrections were conducted using a 0.4-arc-sec digital ellipsoidal height model (DEHM) generated from a Digital Elevation Model (DEM) provided by the Geospatial Information Authority of Japan (GSI). The orbital phase ramp was removed by subtraction of the phase simulated from the precision orbital information. Atmospheric errors, which are caused by variable distributions of water–vapor contents in the troposphere, were reduced by subtracting the elevation-correlated component. For phase unwrapping, we used the SNAPHU algorithm (Chen and Zebker 2002). Finally, the interferograms were geocoded to fit into standard mapping coordinate systems with a pixel spacing of 0.8 arc sec (about 25 m in longitudinal direction and 30 m in latitudinal direction, respectively).

Since we could use the SAR data acquired from four independent directions, it is possible to resolve the 3-D displacement field. We estimated the three components

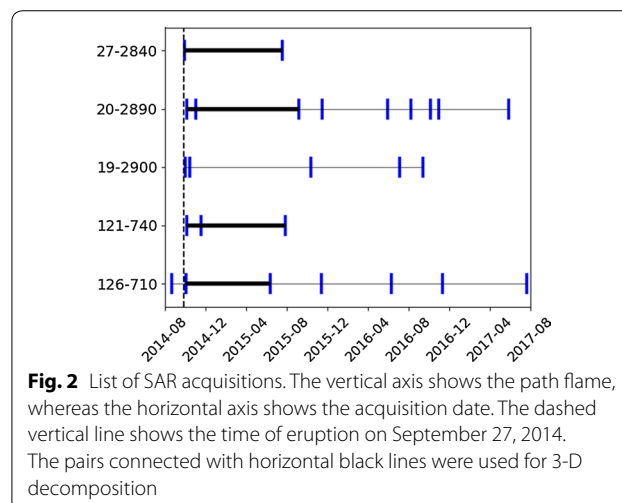
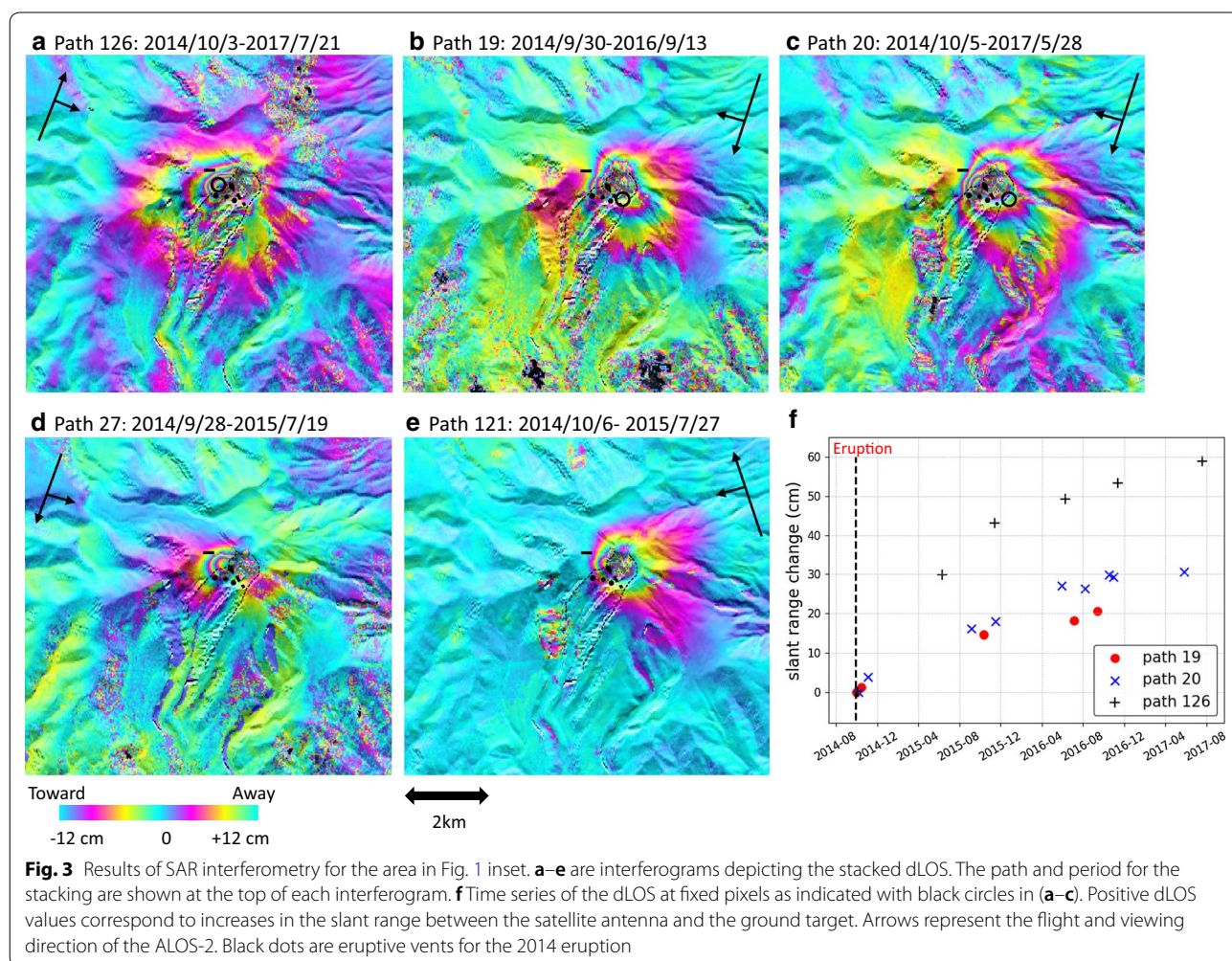


**Fig. 2** List of SAR acquisitions. The vertical axis shows the path flame, whereas the horizontal axis shows the acquisition date. The dashed vertical line shows the time of eruption on September 27, 2014. The pairs connected with horizontal black lines were used for 3-D decomposition

of the displacement at each pixel using four interferograms (Additional file 1: Fig. S1, Table S1). The time span of the interferograms acquired during different periods was rearranged by temporal interpolation so that they represented cumulative deformation during the same period, i.e., from early October 2014 to end of July 2015. During this period, we assumed the displacement velocity was constant. Finally, we obtained the 3-D displacement field using an inversion method developed by Wright et al. (2004). We carried out least square process on a pixel by pixel basis. In this scheme, the observations are corresponding phase values of all the 4 independent interferograms for the same pixel. The sum of atmospheric noise component and decorrelation component was used for the diagonal elements of the covariance matrix as suggested in Morishita et al. (2016), whereas non-diagonal components were zero. A coherence value computed over a small spatial window around the considered pixel was used in the variance estimation process.

### InSAR results

All of the interferograms showed manifestations of positive phase changes around the Jigokudani Valley (Fig. 3). A positive phase change corresponds to an increase in the distance change in line of sight direction (dLOS), suggesting subsidence of the ground surface. The spatial dimensions of the subsided area were about 4 km × 3 km, and dLOS was on the order of decimeters. The center of subsidence was near the eruptive vents. Although the coherence was degraded in some areas, for example, in the Jigokudani Valley itself where the topography is rugged, the overall profile of the fringes clearly indicated deflation at a relatively shallow depth. The high frequency of the data acquisition enabled us to trace the temporal evolution of the deflation (Fig. 3). The deflation began the day after the eruption and continues as of July 2017. The largest dLOS velocity values in coherent areas were 21 cm/year for path 126 and 12 cm/year for path 20, respectively. The temporal profile of the dLOS for the



both paths seemed to be on an exponentially decaying curve.

The 3-D representation of the deformation field derived from decomposition of the displacement field provides a more intuitive representation of the nature of ground deformation. Figure 4 shows the 3-D displacement field between October 2014 and July 2015. The UD and EW component results showed higher signal-to-noise ratios (Fig. 4a, c, d, f). The NS component results were significantly degraded (Fig. 4b, e), as expected due to the near polar orbit of ALOS-2 satellite. Thus, we mostly rely on the EW and UD components in the following discussions. The EW and UD displacement fields resemble the typical displacement pattern of a shallow point deflation source. A typical pattern of a point source deflation was recognizable even in the NS component around the central region (Fig. 4), where the signal-to-noise ratio was relatively good. The spatial dimensions of the deformed region were about 3 km for the UD component and about 4 km for the EW component, respectively. The largest displacement in 10 months was found for the UD component, with a subsidence value as large as 35 cm, whereas the maximum value in the EW component was 22 cm.

### Modeling

To unveil the geometrical structure of the deflation source, we modeled the deformation using both analytical and numerical methods. We began with the analytical modeling of an elastic half-space medium and then built the numerical model, taking into consideration the steep topography of the Ontake Volcano to get a more realistic assessment.

As a first step, we used analytical formulations for a Mogi source (Mogi 1958) and a sill-like horizontal crack source (Okada 1992) in an elastic half-space medium. Horizontal crack models are often used to model ground deformation at shallow volcanic hydrothermal system (e.g., Hamling et al. 2016; Doke et al. 2018; Kobayashi 2018; Kobayashi et al. 2018). Using the EW and UD components, we estimated the horizontal position, depth, and source volume changes by inversion to minimize the sum of the normalized squared residuals. The best-fit solution for the spherical one was a point deflation source at 390 m depth below the eruptive craters (Table 1; Additional file 1: Fig. S2, Table S2). The estimated deflation volume was  $2.9 \times 10^5 \text{ m}^3$  for a 10-month period (Table 1). The residual of the best-fit solution for the crack source was larger than that for the Mogi source, and a relatively large opening was estimated for a small horizontal size crack, both suggesting smaller likelihood of the existence of the source of this kind for this case.

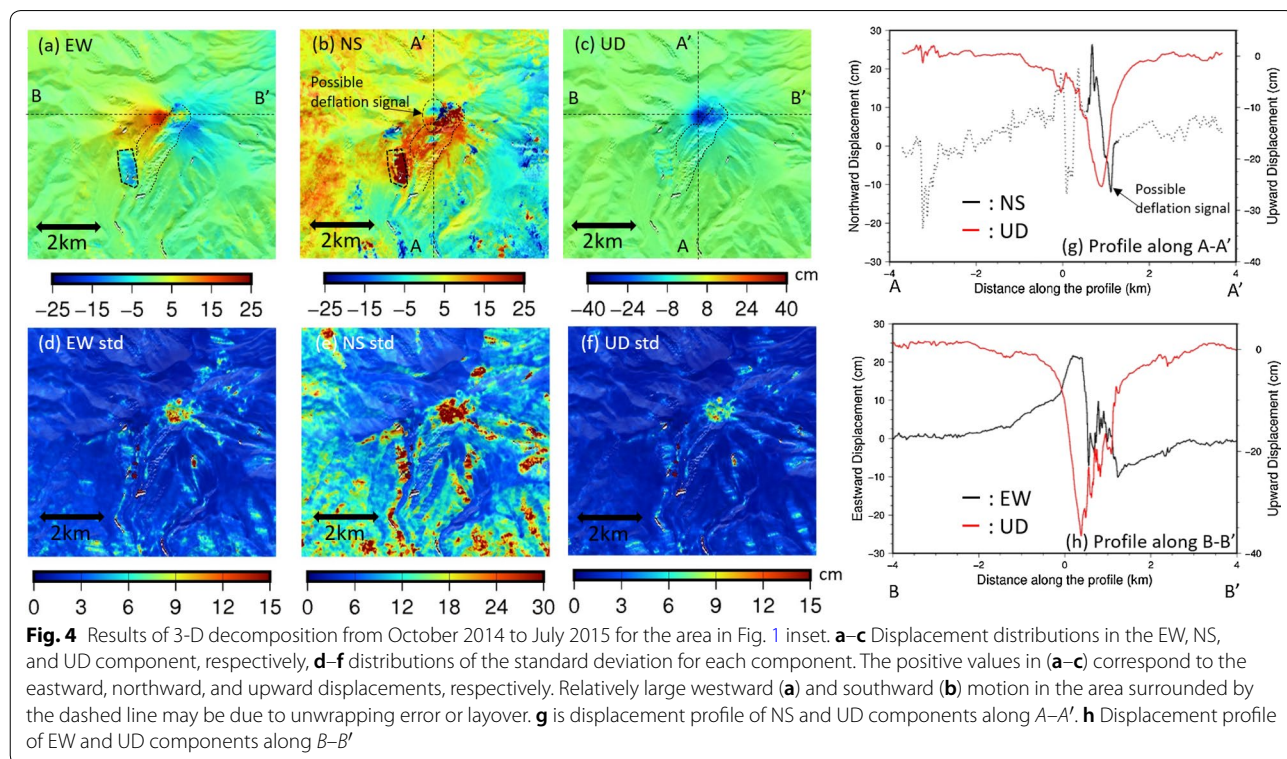


**Table 1 Modeling results**

|                                    | Crack                 | Mogi                  | FEM                   |
|------------------------------------|-----------------------|-----------------------|-----------------------|
| Depth (m)                          | 690                   | 390                   | 500                   |
| Deflation volume (m <sup>3</sup> ) | 3.6 × 10 <sup>5</sup> | 2.9 × 10 <sup>5</sup> | 3.5 × 10 <sup>5</sup> |
| Residual <sup>a</sup>              | 1.80                  | 1.39                  | 0.84                  |

<sup>a</sup> Residual is defined as  $\sqrt{\frac{1}{n} \sum_{i=1}^n \left(\frac{O_i - C_i}{E_i}\right)^2}$  where  $O_i$ ,  $C_i$ , and  $E_i$  are the observed values, calculated values, and observed error values (Fig. 4d–f) at the  $i$ th pixel and  $n$  is the total number of pixels, respectively

To improve the fit, we then built a finite element model (FEM). We employed the Salome-Meca software package (<https://www.code-aster.org>) to (1) take topographic effects into account and (2) to allow flexibility for the source shape. For the topographic data, we used a 0.4-arc-sec DEM generated by GSI. We set the resolution as 20 m in the 4 km × 4 km region around the Jigokudani Valley and 2 km in the outer margin region. The size of the entire model was 26 km × 26 km × 8 km. We placed a spheroidal source with horizontal position fixed to the best-fit position of the Mogi source. The spatial pattern of the deformation appeared axisymmetric. For simplicity, we assumed that one of the axes of the spheroidal source was parallel to the vertical axis (i.e., a non-dipping ellipsoid) and that the spheroid was axisymmetric around

the vertical axis. The major axis of the spheroid was fixed as 200 m. Using grid search, we solved for source depth, which was defined as depth of the center of the spheroid, volume change, and aspect ratio of the spheroidal source as free model parameters. Search range was 300–800 m below surface for source depth and was 0.4–1.0 for source aspect ratio, respectively. The search interval was 100 m for the depth and was 0.1 for the aspect ratio, respectively. The FEM results (Fig. 5) showed that the preferred source shape was almost spherical (aspect ratio: 0.9) at a depth of 500 m below the surface (Fig. 5e). The deflation volume between October 2014 and July 2015 was 3.5 × 10<sup>5</sup> m<sup>3</sup>, and the cumulative volume change through 2017 was 7 × 10<sup>5</sup> m<sup>3</sup> assuming the same temporal profile as that of dLOS change in path 126 (Fig. 3f). Our modeled source was emplaced at a shallower depth than any deformation and seismic sources reported by other authors (Fig. 6) such as the tilt source at 1100 m depth prior to the 2014 eruption (Maeda et al. 2017), the inflation source at 900 m and 3 km depth between 2005 and 2007 (Takagi and Onizawa 2016), the subsidence source at 6 km depth revealed by leveling after the 2014 eruption (Murase et al. 2016) and the VT hypocenters, distributed around 3 km depth (Kato et al. 2015).

We tested our best-fit FEM source using another independent data set. The Japanese Metrological Agency

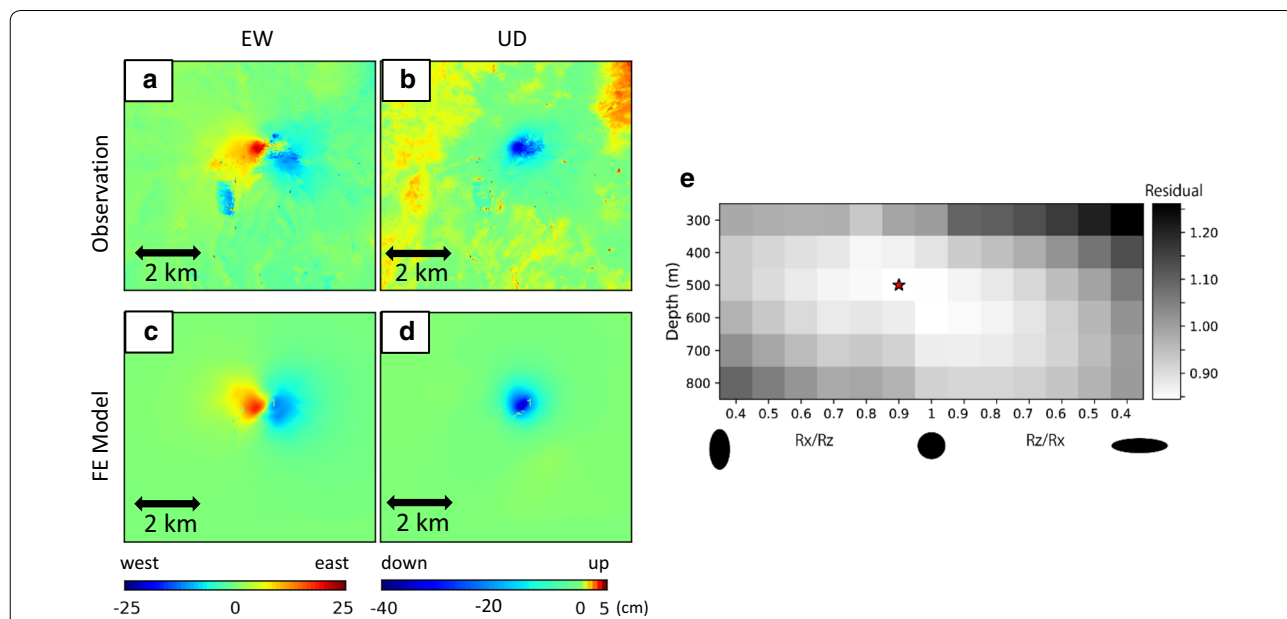
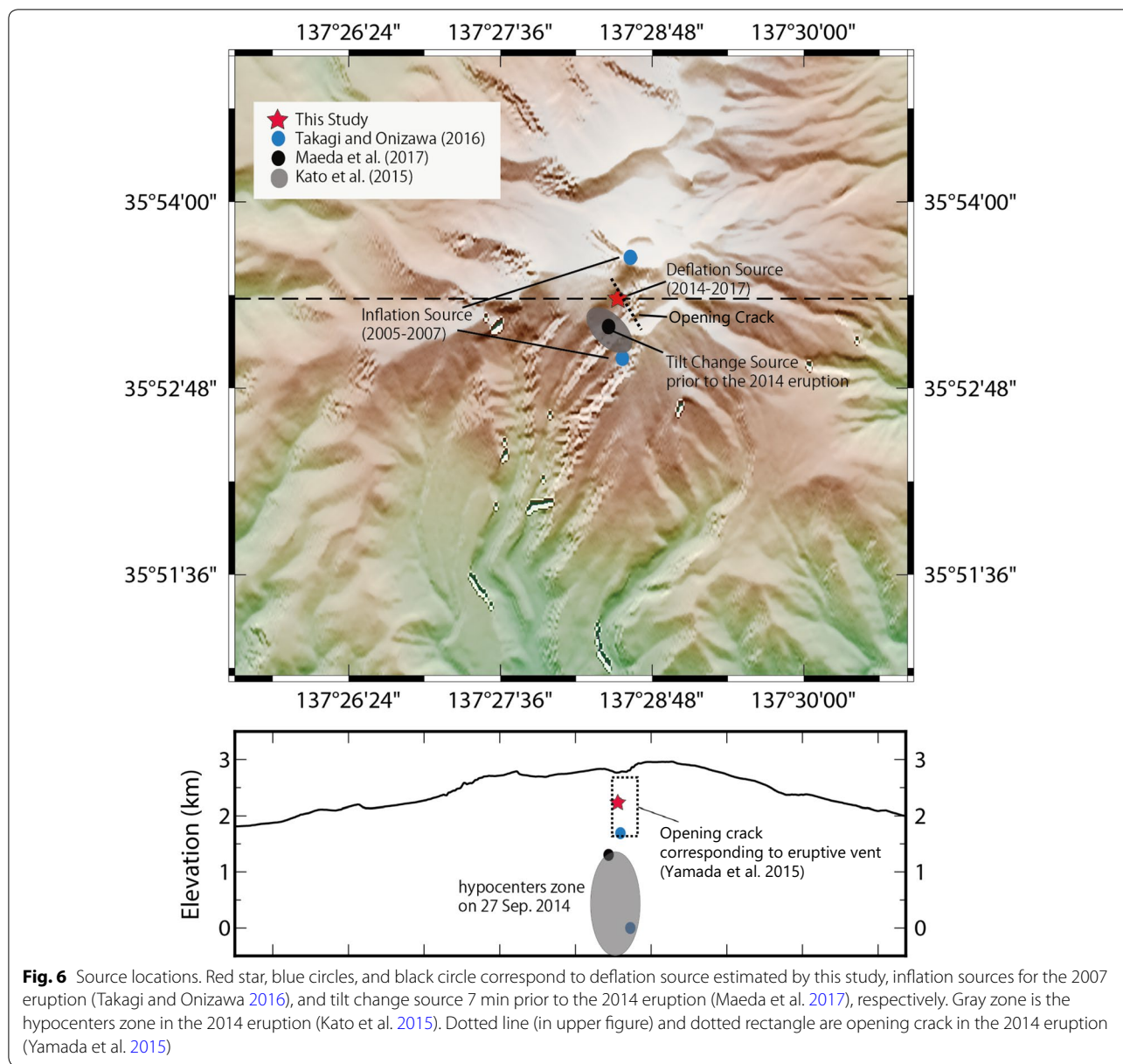
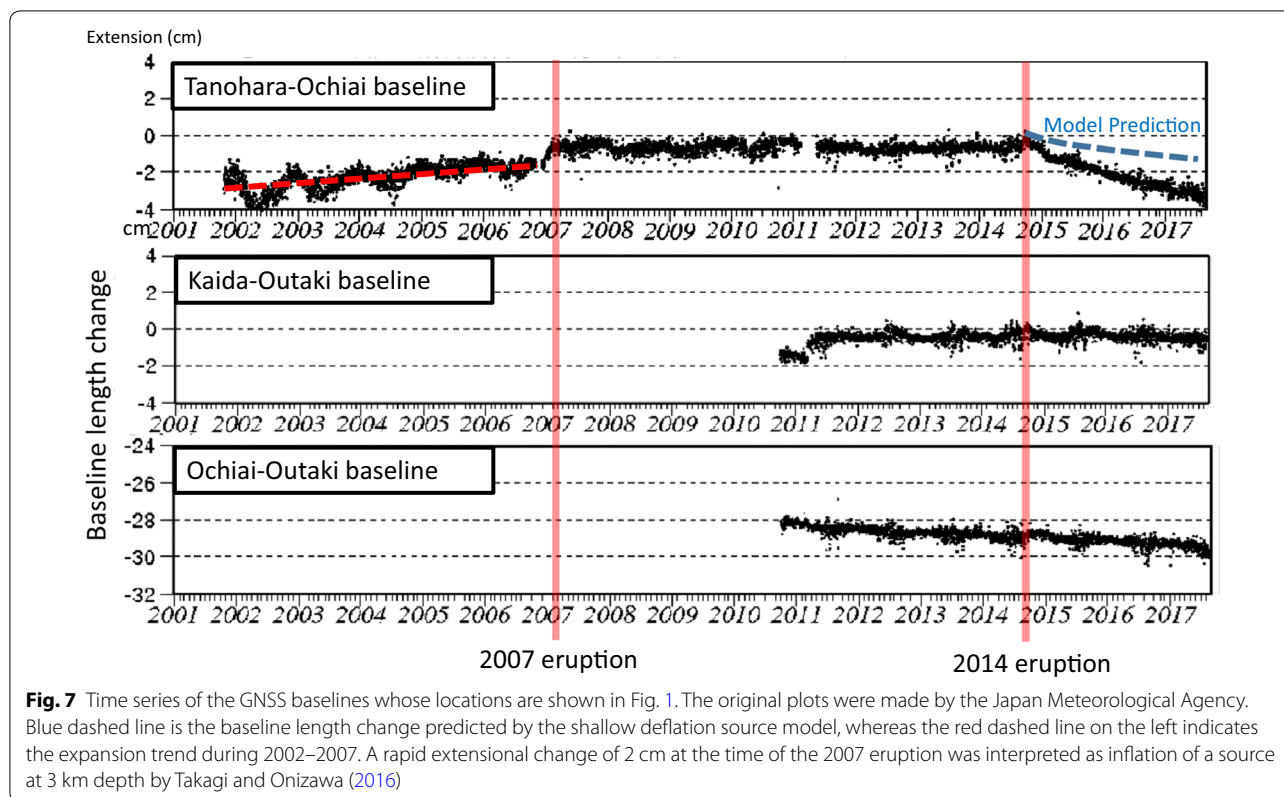


**Fig. 5** Results of FEM modeling for the area in Fig. 1 inset. **a, b** Observations of the EW and UD component are the same as those presented in Fig. 4a, c, respectively. **c, d** Synthesized distributions for the corresponding components based on the best-fit model. **e** Residual distribution for combinations of the free parameters, that is, the aspect ratio of the spheroidal source (abscissa: ratio of the minor axis to the major axis with typical shape schematics) and the depth (ordinate). In the left half of the chart, the aspect ratio is represented as a ratio of the horizontal axis to the vertical axis and the shape is characterized as prolate (vertically elongated), whereas in the right half of the chart, the ratio is for the horizontal axis to the vertical axis and the shape is oblate. The residuals are colored in grayscale. A red star indicates the best-fit combination of the parameters



(JMA) reported baseline changes between GNSS stations deployed around the Ontake Volcano (Fig. 1). They showed that distance changes appeared only in the baseline between the Tanohara and Ochiai Karatani (TO) stations spanning the Ontake Volcano. The TO baseline length contracted by about 2.0 cm during the period between the end of September 2014 and the end of July 2015 (Fig. 7), for which we conducted the FE modeling. There were no significant changes in the other baselines (Fig. 7). We computed the distance change for the TO baseline using the best-fit FE model and found that the expected decrease was 0.7 cm for the modeling period, smaller than the observed 2 cm by 1.3 cm. This

inconsistency implies that another source besides the shallow deflation source found by InSAR could have contributed to the TO baseline contraction, although the possibility of inadequacies in the elastic model remains. Candidates for such a source could be, for example, an inflation source emplaced at 1 km depth between 2005 and 2007 or an inflation source emplaced at 3 km depth during the 2007 eruption (Fig. 6). To evaluate whether such sources can mitigate the inconsistency, we made simple calculations. First, we fixed horizontal position and depth of the sources estimated in Takagi and Onizawa (2016) and calculated deflation volume inducing 1.3-cm contraction in the TO baseline. Then, we



calculated consequent subsidence. A source at 1 km depth should have produced an additional 10-cm subsidence over the Jigokudani Valley, inconsistent with a residual image of UD component (Fig. 8), and this possibility can be ruled out. A source at 3 km depth would have produced an additional subsidence of only 1.8 cm (Fig. 8). Since this amount of subsidence could be masked by the noise in the InSAR images, we cannot rule out the possibility of the existence. Thus, the possibility remains that the deeper source proposed by Takagi and Onizawa (2016) may also have been depressurizing after the 2014 eruption. If this is the case, the situation would be similar to the 2012 phreatic eruptions at Tongariro Volcano in New Zealand, where a shallower subsidence source detected from InSAR data and a deeper source detected by GNSS data were emplaced at 500 m and 2.5 km depths, respectively (Hamling et al. 2016).

**Discussion**

In this section, we discuss behavior of the deflation source, which may be a depressurizing hydrothermal reservoir beneath Jigokudani Valley, by dividing the entire period into three sub-periods, the pre-, syn-, and post-eruptive periods.

**Pre-eruptive period (2002–2014)**

Here, we discuss when the shallow reservoir developed. Our modeling suggests that a shallow reservoir with a volume of at least  $7 \times 10^5 \text{ m}^3$  existed before the 2014 eruption. During the development of a reservoir of this size, there should be pressurization-induced inflation due to fluid accumulation. The reservoir might have formed either slowly over a relatively long time period or might have formed instantaneously in association with certain episodic events. We can suggest four candidates for the inflation period. The first candidate is a small inflation event 1 month prior to the 2014 eruption (Takagi and Onizawa 2016). The second one is syn-eruptive deformation during the 2007 eruption. The third one is slow extensional change from 2002 to 2007. The final one is unknown deformation before 2002 when there are no GNSS data for the TO baseline. The first candidate is an inflation event small enough that it can only be detected by stacking several GNSS baselines data around Ontake Volcano (Miyaoka and Takagi 2016). The absence of extensional change of 1.5 cm in the TO baseline, which is the simulated value from the deflation source model, rules out this possibility (Fig. 7). The second candidate has already been modeled as a spherical inflation source at 3 km depth below Jigokudani Valley (Takagi and Onizawa 2016) and can also be ruled out. From 2002 to 2007



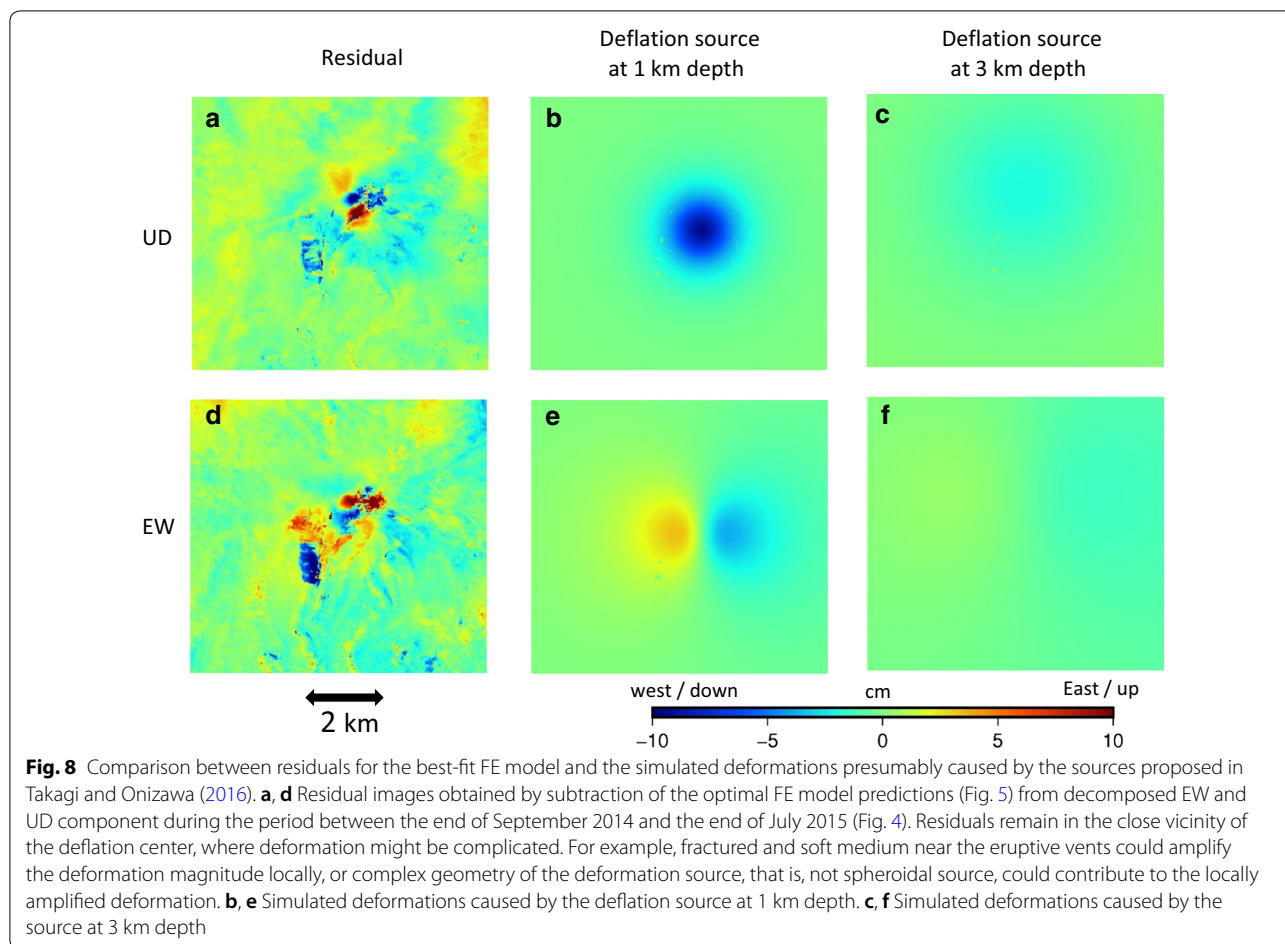


**Fig. 8** Comparison between residuals for the best-fit FE model and the simulated deformations presumably caused by the sources proposed in Takagi and Onizawa (2016). **a, d** Residual images obtained by subtraction of the optimal FE model predictions (Fig. 5) from decomposed EW and UD component during the period between the end of September 2014 and the end of July 2015 (Fig. 4). Residuals remain in the close vicinity of the deflation center, where deformation might be complicated. For example, fractured and soft medium near the eruptive vents could amplify the deformation magnitude locally, or complex geometry of the deformation source, that is, not spheroidal source, could contribute to the locally amplified deformation. **b, e** Simulated deformations caused by the deflation source at 1 km depth. **c, f** Simulated deformations caused by the source at 3 km depth

(third candidate), although there were relatively large seasonal fluctuations, we can recognize a slight baseline extension of about 1 cm. Finally, the fourth possibility cannot be discarded owing to lack of data before 2002. Thus, the shallow reservoir may have formed before 2002 or between 2002 and 2007 and remained stable until the 2014 eruption.

**Syn-eruptive period (08/18/2014–09/29/2014)**

Here, we discuss whether the deflated reservoir was the main source of water and energy for the phreatic eruption on September 27, 2014. Since the deflation began after the eruption, it is natural to suspect that the shallow reservoir was a major source of water and energy. However, this is not the case as suggested below.

First, there was no significant syn-eruptive deflation despite violent fluid discharge such that the eruption plume height reached 10.8 km a.s.l. (Sato et al. 2015). InSAR pair spanning the eruption period (8/18/2014–09/29/2014) showed no net deflation, only a small deformation that was interpreted as opening of a dike-like vertical crack corresponding to vent formation (Yamada

et al. 2015). If most of the discharged water on the first day of the eruption had been provided from the shallow reservoir, syn-eruptive deflation should have manifested in the InSAR data. Unlike the 2014 eruption at Ontake Volcano, phreatic eruptions in 1995 at Kuju Volcano and in 2012 at Tongariro Volcano showed syn-eruptive deflation (Nakaboh et al. 2003; Hamling et al. 2016), which may reflect the rapid depressurization due to fluid discharge. However, the main water source of the 2014 eruption at Ontake Volcano was not the shallow deflated reservoir.

Another consideration is the spatial relationship among the deformation sources, including the crack-like eruptive vent and source of the tilt change immediately before the eruption. This crack-like vent reaches 1 km depth below the Jigokudani Valley (Fig. 6), and this depth is consistent with the source depth of the tilt change, which may have arisen from crack opening due to rapid boiling of liquid water and its subsequent rising to the surface (Maeda et al. 2017). Water and energy for the eruption appeared to be rooted below the shallow reservoir. The shallow reservoir began to depressurize after

**Table 2** Plume mass flux data

| Date       | Mass flux (kg/day) | Data source                                  |
|------------|--------------------|--|
| 09/28/2014 | $2.0 \times 10^8$  | Terada (2014)                                |
| 10/07/2014 | $5.5 \times 10^7$  | Terada (2014)                                |
| 10/10/2014 | $6.0 \times 10^7$  | Terada, personal communication               |
| 11/19/2014 | $6.1 \times 10^7$  | Terada, personal communication               |
| 11/21/2014 | $7.2 \times 10^7$  | Hashimoto and Tanaka, personal communication |
| 11/22/2014 | $5.1 \times 10^7$  | Hashimoto and Tanaka, personal communication |

All estimates are based on plume rise method (Kagiya 1978)

the eruption and was heated by hot fluid ascending from greater depth. The shallow source may not have been involved in the eruption.

These inferences are also consistent with volcanic gas observations. The  $\text{SO}_2$  flux observed on September 28, 2014, was 2500 ton/day, and this amount is too large to be explained by supply from a shallow and isolated hydrothermal reservoir (Mori et al. 2016). It is more reasonable to infer that the discharged fluid at the beginning of the eruption came from a deeper, magmatic region as inferred by Mori et al. (2016).

#### Post-eruptive period (09/30/2014–07/21/2017)

Post-eruptive deflation began after the 2014 eruption, and plume discharge has also continued (Yamaoka et al. 2016). Deflation caused by fluid discharge is typical at volcanoes and geothermal fields (e.g., Lu et al. 2002; Nakaboh et al. 2003; Hamling et al. 2016; Barbour et al. 2016; Juncu et al. 2017).

Since there are estimates of discharge mass (e.g., Terada 2014) as well as deflated volume, we can check simple mass balance between the discharge plume and mass loss corresponding to the deflated volume. Discharge mass flux was previously estimated only for 2 months after the 2014 eruption using images of discharge plume (Table 2). Cumulative mass of the plume ( $Q_{\text{out}}$ ) during that period was  $4 \times 10^9$  kg given by linear interpolation of the mass flux. Deflation volume for the same period ( $dV$ ) is about  $8.8 \times 10^4$  m<sup>3</sup> based on linear interpolation from the deflation volume of  $3.5 \times 10^5$  m<sup>3</sup> between October 2014 and July 2015. If we assume that discharged water is incompressible and its density ( $\rho$ ) is 1000 kg/m<sup>3</sup>, mass loss ( $dm = \rho dV$ ) can be calculated as  $8.8 \times 10^7$  kg. Ratio of the  $dm/Q_{\text{out}}$  was at most  $2.2 \times 10^{-2}$ , which implies that the shallow reservoir could not supply all the discharged water. If this is true, another water source needs to be considered, possibly from a greater depth. This result is very similar to the case of the 1995 eruption at Kuju Volcano, where  $dm/Q_{\text{out}}$  is  $5.6 \times 10^{-2}$  (Nakaboh et al. 2003).

However, the depressurizing hydrothermal reservoir is likely in a two-phase liquid–vapor state. Two-phase water can be no longer approximated as incompressible

fluid but rather is extremely compressible (Grant and Sorey 1979). Furthermore, Segall (2010) points out that fluid compressibility is a key parameter in calculating mass change corresponding to volume changes estimated by geodetic modeling. More realistic estimation of the mass balance needs to take the two-phase water compressibility into account.

#### Conclusion

ALOS-2 InSAR data map deflation following the phreatic eruption in 2014 at Ontake Volcano. The deflation source appears to be a shallow depressurizing hydrothermal reservoir. This reservoir might not be the main source of water and energy for the phreatic eruption that caused violent ejections of rock. GNSS data for pre-eruptive period suggest that the reservoir may have been developed between 2002 and 2007 or even before 2002. The quantitative relationship between ongoing post-eruptive deflation and plume discharge remains unclear due to the complexity of pressure transmission in an evolving two-phase system.

#### Additional file

**Additional file 1. Fig. S1.** The InSAR pairs used for estimation of the 3-D deformation field. The key parameters of used pairs are described in Table S1. The pair numbers correspond to those of Table S1. **Fig. S2** Deformation patterns of best-fit analytical models. Parameters of the optimal solutions are shown in Table S2. **Table S1** InSAR data used for estimating the 3-D displacement field. **Table S2** Optimal parameters of analytical and finite element models.

#### Authors' contributions

SN performed InSAR analysis and source modeling and wrote the manuscript. SN and MM interpreted the InSAR results and drew the conclusions. Both authors read and approved the final manuscript.

#### Author details

<sup>1</sup> Department of Natural History Sciences, Graduate School of Science, Hokkaido University, N10W8, Kita-ku, Sapporo, Hokkaido 060-0810, Japan. <sup>2</sup> Institute of Seismology and Volcanology, Faculty of Science, Hokkaido University, N10W8, Kita-ku, Sapporo, Hokkaido 060-0810, Japan.

### Acknowledgements

We thank editor Tomokazu Kobayashi, Dr. Steve Ingebritsen, and an anonymous reviewer for their valuable comments to improve the quality of our manuscript. We are grateful to Dr. Tomofumi Kozono and Dr. Ryo Tanaka for valuable discussion with them. We appreciate Dr. Akihiko Terada, Prof. Takeshi Hashimoto, and Dr. Ryo Tanaka allowing us to use unpublished data of the plume mass flux. We thank Dr. Taku Ozawa for providing RINC to conduct InSAR analysis. We analyzed ALOS-2/PALSAR-2 data which are shared within the PALSAR Interferometry Consortium to Study our Evolving Land Surface (PIXEL). ALOS-2/PALSAR-2 data were provided by the Japan Aerospace Exploration Agency (JAXA) under a cooperative research contract with the Earthquake Research Institute (ERI) at the University of Tokyo. The ownership of the original PALSAR-2 data belongs to JAXA. The data were provided through PIXEL and working group of Coordinating Committee for Prediction of Volcanic Eruption. We used 10-m-mesh DEM published by Geospatial Information Authority of Japan. We used the Generic Mapping Tools (Wessel and Smith 1998) and matplotlib (Hunter 2007) for drawing the figures.

### Competing interests

The authors declare that they have no competing interests.

### Availability of data and materials

All the interferograms presented here were generated from ALOS-2/PALSAR-2 level 1.1 data, which can be purchased through RESTEC ([www.restec.or.jp](http://www.restec.or.jp)) or PASCO ([www.pasco.co.jp](http://www.pasco.co.jp)).

### Funding

This study was supported by the Ministry of Education, Culture, Sports, Science and Technology (MEXT) of Japan, under its Earthquake and Volcano Hazards Observation and Research Program (Grant No. 1008).

### Publisher's Note

Springer Nature remains neutral with regard to jurisdictional claims in published maps and institutional affiliations.

Received: 8 June 2018 Accepted: 29 November 2018

Published online: 11 December 2018

### References

- Barbour A, Evans E, Hickman S, Eneva M (2016) Subsidence rates at the southern Salton Sea consistent with reservoir depletion. *J Geophys Res* 121:5308–5327. <https://doi.org/10.1002/2016JB012903>
- Chen C, Zebker H (2002) Phase unwrapping for large SAR interferograms: statistical segmentation and generalized network models. *IEEE Trans Geosci Remote Sens* 40:1709–1719. <https://doi.org/10.1109/TGRS.2002.802453>
- Currenti G, Napoli R, Coco A, Privitera E (2017) Effects of hydrothermal unrest on stress and deformation: insights from numerical modeling and application to Vulcano Island (Italy). *Bull Volcanol* 79:28. <https://doi.org/10.1007/s00445-017-1110-3>
- Doke R, Harada M, Mannen K, Itadera K, Takenaka J (2018) InSAR analysis for detecting the route of hydrothermal fluid to the surface during the 2015 phreatic eruption of Hakone Volcano, Japan. *Earth Planets Space* 70:63. <https://doi.org/10.1186/s40623-018-0834-4>
- Fournier N, Chardot L (2012) Understanding volcano hydrothermal unrest from geodetic observations: insights from numerical modeling and application to White Island Volcano, New Zealand. *J Geophys Res* 117:B11208. <https://doi.org/10.1029/2012JB009469>
- Grant M, Sorey M (1979) The compressibility and hydraulic diffusivity of a water-steam flow. *Water Resour Res* 15:684–686. <https://doi.org/10.1029/WR015i003p00684>
- Hamling I, Williams C, Hreinsdóttir S (2016) Depressurization of a hydrothermal system following the August and November 2012 Te Maari eruptions of Tongariro, New Zealand. *Geophys Res Lett* 43:168–175. <https://doi.org/10.1002/2015GL067264>
- Hunter J (2007) Matplotlib: a 2D graphics environment. *Comput Sci Eng* 9:90–95. <https://doi.org/10.1109/MCSE.2007.55>
- Ingebritsen SE, Shelly DR, Hsieh PA, Clor LE, Seward PH, Evans WC (2015) Hydrothermal response to a volcano-tectonic earthquake swarm, Lassen, California. *Geophys Res Lett* 42:9223–9230. <https://doi.org/10.1002/2015GL065826>
- Juncu D, Árnadóttir T, Hooper A, Gunnarsson G (2017) Anthropogenic and natural ground deformation in the Hengill geothermal area, Iceland. *J Geophys Res Solid Earth* 122:692–709. <https://doi.org/10.1002/2016JB013626>
- Kagiyama T (1978) Evaluation of heat discharge and H<sub>2</sub>O emission from volcanoes-based on a plume rise assumption. *Bull Volcanol Soc Jpn* 23:183–197 (in Japanese with English abstract)
- Kato A, Terakawa T, Yamanaka Y, Maeda Y, Horikawa S, Matsuhiro K, Okubo T (2015) Preparatory and precursory processes leading up to the 2014 phreatic eruption of Mount Ontake, Japan. *Earth Planets Space* 67:1–11. <https://doi.org/10.1186/s40623-015-0288-x>
- Kobayashi T (2018) Locally distributed ground deformation in an area of potential phreatic eruption, Midagahara Volcano, Japan, detected by single-look-based InSAR time series analysis. *J Volcanol Geotherm Res* 357:213–223. <https://doi.org/10.1016/j.jvolgeores.2018.04.023>
- Kobayashi T, Morishita Y, Munekane H (2018) First detection of precursory ground inflation of a small phreatic eruption by InSAR. *Earth Planet Sci Lett* 491:244–254. <https://doi.org/10.1016/j.epsl.2018.03.041>
- Lu Z, Masterlark T, Power J, Dzurisin D, Wicks C (2002) Subsidence at Kiska Volcano, Western Aleutians, detected by satellite radar interferometry. *Geophys Res Lett* 29:2-1–2-4. <https://doi.org/10.1029/2002gl014948>
- Maeda Y, Kato A, Yamanaka Y (2017) Modeling the dynamics of a phreatic eruption based on a tilt observation: barrier breakage leading to the 2014 eruption of Mount Ontake, Japan. *J Geophys Res* 122:1007–1024. <https://doi.org/10.1002/2016JB013739>
- Miller C, Currenti G, Hamling I, Williams-Jones G (2018) Mass transfer processes in a post eruption hydrothermal system: parameterisation of microgravity changes at Te Maari craters, New Zealand. *J Volcanol Geotherm Res* 357:39–55. <https://doi.org/10.1016/j.jvolgeores.2018.04.005>
- Minami Y, Imura T, Hayashi S, Ohba T (2016) Mineralogical study on volcanic ash of the eruption on September 27, 2014 at Ontake Volcano, Central Japan: correlation with porphyry copper systems. *Earth Planets Space* 68:67. <https://doi.org/10.1186/s40623-016-0440-2>
- Miyaoka K, Takagi A (2016) Detection of crustal deformation prior to the 2014 Mt. Ontake eruption by the stacking method. *Earth Planets Space* 68:60. <https://doi.org/10.1186/s40623-016-0439-8>
- Mogi K (1958) Relations between the eruptions of various volcanoes and the deformations of the ground surfaces around them. *Bull Earthq Res Inst* 36:99–134
- Mori T, Hashimoto T, Terada A, Yoshimoto M, Kazahaya R, Shinohara H, Tanaka R (2016) Volcanic plume measurements using a UAV for the 2014 Mt. Ontake eruption. *Earth Planets Space* 68:49. <https://doi.org/10.1186/s40623-016-0418-0>
- Morishita Y, Kobayashi T, Yurai H (2016) Three-dimensional deformation mapping of a dike intrusion event in Sakurajima in 2015 by exploiting the right- and left-looking ALOS-2 InSAR. *Geophys Res Lett* 43:4197–4204. <https://doi.org/10.1002/2016GL068293>
- Murase M, Kimata F, Yamanaka Y, Horikawa S, Matsuhiro K, Matsushima T, Mori H, Ohkura T, Yoshikawa S, Miyajima R, Inoue H, Mishima T, Sonoda T, Uchida K, Yamamoto K, Nakamichi H (2016) Preparatory process preceding the 2014 eruption of Mount Ontake Volcano, Japan: insights from precise leveling measurements. *Earth Planets Space* 68:9. <https://doi.org/10.1186/s40623-016-0386-4>
- Nakaboh M, Ono H, Sako M, Sudo Y, Hashimoto T, Hurst AW (2003) Continuing deflation by fumaroles at Kujū Volcano, Japan. *Geophys Res Lett*. <https://doi.org/10.1029/2002gl016047>
- Nakamichi H, Kumagai H, Nakano M, Okubo M, Kimata F, Ito Y, Obara K (2009) Source mechanism of a very-long-period event at Mt. Ontake, Central Japan: response of a hydrothermal system to magma intrusion beneath the summit. *J Volcanol Geotherm Res* 187:167–177. <https://doi.org/10.1016/j.jvolgeores.2009.09.006>
- Okada Y (1992) Internal deformation due to shear and tensile faults in a half-space. *Bull Seismol Soc Am* 82:1018–1040
- Oikawa T (2008) Reinvestigation of the historical eruption and fumarolic activity records at Ontake Volcano, central Japan. Misunderstanding reports about the 774 AD and (1892) AD eruptions. *Bull Geol Surv Japan* 59(5–6):203–210
- Ozawa T, Fujita E, Ueda H (2016) Crustal deformation associated with the 2016 Kumamoto Earthquake and its effect on the magma system of

- Aso Volcano. *Earth Planets Space* 68:186. <https://doi.org/10.1186/s40623-016-0563-5>
- Rouwet D, Sandri L, Marzocchi W, Gottsmann J, Selva J, Tonini R, Papale P (2014) Recognizing and tracking volcanic hazards related to non-magmatic unrest: a review. *J Appl Volcanol* 3:17. <https://doi.org/10.1186/s13617-014-0017-3>
- Sato E, Shinbori T, Fukui K, Ishii K, Takagi A (2015) The eruption cloud echo from Mt. Ontake on September 27, 2014 observed by weather radar network. Report of Coordinating Committee for Prediction of Volcanic Eruptions, no. 119
- Segall P (2010) Earthquake and volcano deformation. Princeton University Press, Princeton, pp 212–213
- Takagi A, Onizawa S (2016) Shallow pressure sources associated with the 2007 and 2014 phreatic eruptions of Mt. Ontake, Japan. *Earth Planets Space* 68:135. <https://doi.org/10.1186/s40623-016-0515-0>
- Takarada S, Oikawa T, Furukawa R, Hoshizumi H, Itoh J, Geshi N, Miyagi I (2016) Estimation of total discharged mass from the phreatic eruption of Ontake Volcano, Central Japan, on September 27, 2014. *Earth Planets Space* 68:138. <https://doi.org/10.1186/s40623-016-0511-4>
- Tanaka R, Hashimoto T, Matsushima N, Ishido T (2017) Permeability-control on volcanic hydrothermal system: case study for Mt. Tokachidake, Japan, based on numerical simulation and field observation. *Earth Planets Space* 69:39. <https://doi.org/10.1186/s40623-017-0623-5>
- Terada A (2014) Heat discharge activities from the Jigokudani Crater at Ontake Volcano after the phreatic eruption in September 2014. In: 2014 fall meeting of Volcanological Society of Japan, UP-24 (in Japanese)
- Wessel P, Smith WHF (1998) New, improved version of generic mapping tools released. *EOS Trans Am Geophys Union* 79:579
- Wright T, Parsons B, Lu Z (2004) Toward mapping surface deformation in three dimensions using InSAR. *Geophys Res Lett.* <https://doi.org/10.1029/2003gl018827>
- Yamada S, Morishita Y, Wada K, Kikkawa T, Yamanaka M, Fujiwara S, Tobita M, Yagai H, Kobayashi T (2015) Detection of deformation triggered by eruption of Mt. Ontake Volcano with InSAR using ALOS-2 data. *J Geospat Inf Auth Jpn* 127:11–15
- Yamaoka K, Geshi N, Hashimoto T, Ingebritsen SE, Oikawa T (2016) Special issue "The phreatic eruption of Mt. Ontake Volcano in 2014". *Earth Planets Space* 68:175. <https://doi.org/10.1186/s40623-016-0548-4>

Submit your manuscript to a SpringerOpen® journal and benefit from:

- Convenient online submission
- Rigorous peer review
- Open access: articles freely available online
- High visibility within the field
- Retaining the copyright to your article

---

Submit your next manuscript at ► [springeropen.com](http://springeropen.com)

---